




# Creation of silicon vacancy color centers with a narrow emission line in nanodiamonds by ion implantation

HIDEAKI TAKASHIMA,<sup>1,6</sup>  ATSUSHI FUKUDA,<sup>1,6</sup> KONOSUKE SHIMAZAKI,<sup>1,6</sup> YUSUKE IWABATA,<sup>2,6</sup> HIROKI KAWAGUCHI,<sup>1</sup> ANDREAS W. SCHELL,<sup>3,4</sup>  TOSHIYUKI TASHIMA,<sup>1</sup>  HIROSHI ABE,<sup>5</sup>  SHINOBU ONODA,<sup>5</sup> TAKESHI OHSHIMA,<sup>5</sup>  AND SHIGEKI TAKEUCHI<sup>1,\*</sup> 

<sup>1</sup>Department of Electronic Science and Engineering, Kyoto University, Kyotodaigakusura, Nishikyo-ku, Kyoto 615-8510, Japan

<sup>2</sup>Undergraduate School of Electrical and Electronic Engineering, Kyoto University, Kyotodaigakusura, Nishikyo-ku, Kyoto 615-8510, Japan

<sup>3</sup>Institut für Festkörperphysik, Leibniz Universität Hannover, 30167 Hannover, Germany

<sup>4</sup>Physikalisch-Technische Bundesanstalt, 38116 Braunschweig, Germany

<sup>5</sup>Takasaki Advanced Radiation Research Institute, National Institutes for Quantum and Radiological Science and Technology, 1233 Watanuki, Takasaki, Gunma 370-1292, Japan

<sup>6</sup>These authors contributed equally to this work  
[takeuchi@kuee.kyoto-u.ac.jp](mailto:takeuchi@kuee.kyoto-u.ac.jp)

**Abstract:** Nanodiamonds containing silicon-vacancy (SiV) centers with high brightness, high photo-stability, and a narrow zero phonon line (ZPL) have attracted attention for bioimaging, nanoscale thermometry, and quantum technologies. One method to create such nanodiamonds is the milling of diamond films synthesized by chemical vapor deposition (CVD). However, this requires post-processing such as acid treatment and centrifugation after the milling process. Therefore, the number of SiV center-containing nanodiamonds made from an initial CVD diamond is small. An alternative method without these problems is the implantation of Si ions into preselected nanodiamonds. This method, however, has an issue regarding the ZPL linewidths, which are more than twice as broad as those in nanodiamonds synthesized by CVD. In order to reduce the linewidth, we employed annealing treatment at high temperatures (up to 1100 °C) and high vacuum after the implantation. For an ion fluence of  $10^{13}$  ions/cm<sup>2</sup>, a ZPL with a linewidth of about 7 nm at room temperature was observed for a nanodiamond with a median size of  $29.9 \pm 16.0$  nm. This was close to the linewidth for nanodiamonds created by CVD.

© 2021 Optical Society of America under the terms of the [OSA Open Access Publishing Agreement](#)

## 1. Introduction

Nanodiamonds containing color centers have attracted attention recently for applications in biological science [1,2], quantum sensing [3–5], and quantum information processing [6,7]. In various color centers, silicon vacancy (SiV) centers have especially promising properties, with high photo-stability and high brightness [8]. About 70% of the photons are emitted into a zero phonon line (ZPL) at about 737 nm in biological windows [8,9]. SiV centers exhibit a lifetime-limited fluorescence linewidth and no spectral diffusion [10–12]. They also exhibit nonblinking with nearly lifetime-limited linewidths [13]. SiV centers enable the emission of indistinguishable photons from separate emitters [9,12]. In addition, the electronic spin of a SiV center is optically accessible [14–17]. Recently, bright single-photon emitting diode has been proposed [18] and integration with diamond-based nanophotonic devices has been demonstrated [19,20]. SiV centers in nanodiamonds are also interesting for biomarkers in the near infrared

region and integration with nanophotonic devices, such as photonic crystal cavities [21,22], optical nanofibers [23–27], and nanofiber Bragg cavities [28–32], using bottom-up techniques [33]. It is noted that narrow linewidths of ZPLs in nanodiamonds at room temperature are important for room-temperature sensing applications, such as all-optical thermometry [34] and cathodoluminescence (CL) imaging [35]. For all-optical thermometry, the peak shift of the ZPL of SiV centers was used for the thermometry and thus the linewidth at room temperature matters [34]. For CL imaging, it is desirable to use SiV centers with spectrally narrow fluorescence peaks as cathodoluminescence markers, in order to distinguish them from the CL background [35].

One method for fabricating nanodiamonds including SiV centers is the milling of nanocrystalline diamond film synthesized by chemical vapor deposition (CVD) [36,37]. In this method, the achieved high crystalline quality generates a narrow ZPL linewidth at room temperature (5–17 nm) [36,37]. However, this method requires complicated post-processing, such as acid treatment cleaning and centrifugation for size selection, after a milling process, such as bead-assisted sonic disintegration (BASD) [36] and wet-milling [37]. As a result, the number of SiV-containing nanodiamonds made from an initial CVD diamond is small. An alternative method to directly produce nanometer- and micrometer-sized crystals with SiV centers is the synthesis of high-pressure high-temperature (HPHT) [38,39].

Another alternative method is ion implantation into preselected nanodiamonds with uniform size. This method makes it possible to create SiV centers in uniform nanodiamonds without milling and the subsequent post-processing after forming SiV centers. However, one issue with Si-implanted nanodiamonds is the broad linewidth for the ZPLs [40,41]. SiV centers have been created in 40 nm nanodiamonds by implanting Si ions at a fluence of  $10^{17}$  ions/cm<sup>2</sup> [40]. They have also been created in nanodiamonds of 15 nm size by implanting Si ions at a high acceleration voltage (2.3 MeV) [41]. The observed linewidths in these studies were about 16 nm at room temperature. These were more than twice as broad as those of SiV centers in nanodiamonds synthesized by CVD [36,37,40,42]. Therefore, it is important to develop a method to reduce the linewidth for the ZPL of SiV centers in nanodiamonds implanted with ions.

In this paper, we report the creation of SiV centers with narrow ZPL linewidths in nanodiamonds by ion implantation and annealing treatment at high temperature (up to 1100°C) and high vacuum [43]. Si ions are implanted into nanodiamonds with different median sizes of  $29.9 \pm 16.0$  nm,  $53.7 \pm 11.2$  nm, and  $65.7 \pm 28.8$  nm while changing the ion fluence from  $10^{11}$  ions/cm<sup>2</sup> to  $2 \times 10^{15}$  ions/cm<sup>2</sup>. For an ion fluence of  $10^{13}$  ions/cm<sup>2</sup>, SiV centers with a narrow ZPL of about 6 nm at room temperature are observed for nanodiamonds with a median size of  $65.7 \pm 28.8$  nm. This linewidth is more than twice as narrow as the previously observed linewidth for Si-implanted nanodiamonds [40,41] and almost comparable to that of nanodiamonds created by CVD synthesis [36,37]. For nanodiamonds with a median size of  $29.9 \pm 16.0$  nm, we observe a similarly narrow ZPL (about 7 nm).

This paper is organized as follows. Section 2 explains sample preparation. Section 3 describes the experimental setup. In Section 4.1, emission linewidths for SiV centers created in the nanodiamonds are discussed. In Section 4.2, the number of SiV centers in a nanodiamond is estimated. Finally, Section 5 concludes the paper.

## 2. Sample preparation

We use three kinds of type-Ib diamond monocrystalline suspension (MSY 0–0.05, MSY 0–0.1, MSY 0–0.5, purchased from Microdiamant), denoted as samples A, B, and C, respectively. The suspensions are purified by a centrifuge (at 14000 rpm for 30 minutes) to remove fluorescent contaminants. They are then dispersed into ultra-pure water. Small amounts of this solution are spin-coated on cleaned silicon substrates with a thermally oxidized layer (2 μm SiO<sub>2</sub> layer on Si substrate).

We then implant  $^{28}\text{Si}$  ions into the samples. The energies of the implantation into samples A and B are 30 keV. The estimated penetration depth of the ions using Stopping and Range of Ions in Matter (SRIM) is 22 nm. The energy of implantation into sample C is 180 keV and the estimated penetration depth is 120 nm. Ion fluence of  $10^{11}$  ions/cm $^2$ ,  $10^{13}$  ions/cm $^2$ , and  $2 \times 10^{15}$  ions/cm $^2$  are used.

We anneal the implanted samples in high vacuum [43]. After evacuating the sample chamber to under about  $1 \times 10^{-4}$  Pa using a turbomolecular pump, the samples are baked for 4 hours at 400°C. After baking, the temperature is increased to 800°C for 11 hours and then the samples are annealed at 800°C for 8 hours, due to an increased mobility of vacancies. After the temperature returns to room temperature, the samples are heated at 520°C for about 2 hours in air to remove the  $\text{sp}^2$  carbon layer and other contamination on the surface. Next, the samples are again baked at 400°C for 4 hours in vacuum. After this baking, the temperature is increased to 1100°C for 20 hours and the samples are then annealed at this temperature for 2 hours. After this process, the samples are again heated at 520°C for about 2 hours in air to remove  $\text{sp}^2$  carbon and the surface contamination. To observe the samples using an oil-immersion objective lens with high numerical aperture (NA), the nanodiamonds are transferred from the silicon substrate to a microscope cover slip using scotch tape and heated at 520°C for about 1 hour in air to remove the tape residue [44].

We observe the samples using a scanning electron microscopy (SEM) (JEOL-6500F, JEOL Ltd.). The ion fluence of the samples is  $10^{11}$  ions/cm $^2$ . A gold film of about 10 nm thickness is coated on each sample to prevent charging during the observation. The acceleration voltage of the electrons is 5 kV. Figure 1(a) is an SEM image of sample A. Nanodiamonds with a size of about 35 nm (white arrows) were identified in the measured area. The average size of measured 107 nanodiamonds was  $29.9 \pm 16.0$  nm (Table 1). Figure 1(b) is an SEM image of sample B. Nanodiamonds with a size of about 55 nm (white arrows) were observed in the observed area. The average size of measured 29 nanodiamonds was  $53.7 \pm 11.2$  nm. Figure 1(c) shows an SEM image of sample C. Nanodiamonds with a size of about 70 nm (white arrows) were observed with a lower density than in the other samples. The average size of measured 68 nanodiamonds was  $65.7 \pm 28.8$  nm. Note that this size is almost agreement with the size of the nanodiamonds ( $61.3 \pm 20.3$  nm) without our thermal treatment in the suspension purified by the centrifuge.

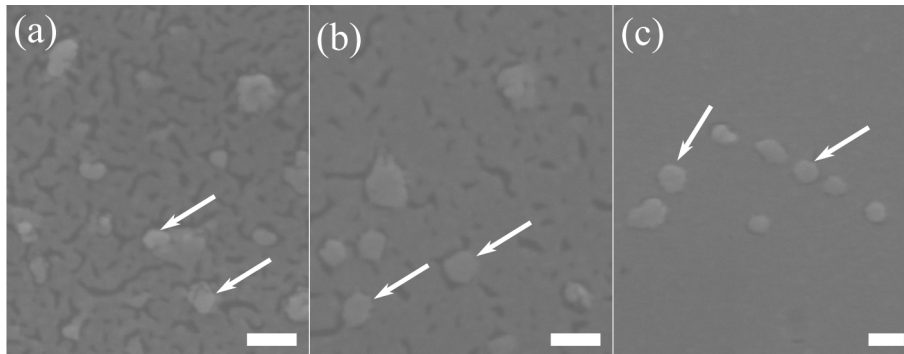


**Fig. 1.** SEM images of sample (a) A, (b) B, and (c) C. Scale bars are 100 nm.

**Table 1. Overview of the investigated nanodiamonds.**

Sample name	A	B	C
Measured median size (nm)	29.9	53.7	65.7
Measured standard deviation (nm)	$\pm 16.0$	$\pm 11.2$	$\pm 28.8$
Energy (keV)	30	30	180
Penetration depth (nm)	22	22	120
Ion fluence (ions/cm <sup>2</sup> )	$10^{11}$ , $10^{13}$ , and $2 \times 10^{15}$ for all samples		

### 3. Experimental setup

The experimental setup consists of a stage scanning confocal microscope as shown in Fig. 2. A continuous-wave laser ( $\lambda = 685$  nm) is used to excite the SiV centers in the nanodiamonds. The excitation power of the laser is about 3.5 mW before the microscope. The laser is passed through a band pass filter of 685 nm (bandwidth  $\sim 10$  nm) and a low pass filter with a cutoff of 715 nm. The laser beam is reflected by a dichroic mirror and focused on the nanodiamonds with an oil-immersion objective lens with a numerical aperture of 1.4. The samples are scanned at a step size of 200 nm using a three-axis piezo actuator. The size of the scanning area is  $10 \mu\text{m} \times 10 \mu\text{m}$ . The fluorescence is collected with the same objective lens and imaged onto a multimode optical fiber (core diameter of about  $10 \mu\text{m}$ ) after passing through the dichroic mirror and optical filters. To obtain confocal scanning images and emission spectra, the light passing through the optical fiber is measured by a single-photon counting module and a spectrometer (Oriel, MS257) equipped with a charge coupled device (CCD) camera (Andor DU4200E). By inserting a flip mirror behind a beam splitter, a second-order correlation function  $g^2(\tau)$  is also measured. In order to measure parts of uniformly distributed nanodiamonds, the regions where the nanodiamonds are thinly dispersed are selected for observation with an optical microscope. The experiments are performed at room temperature.

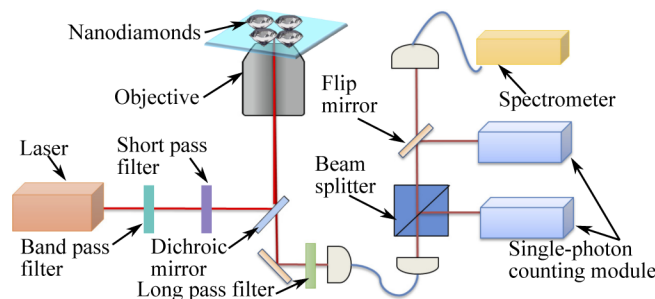


**Fig. 2.** Experimental setup. Laser light is focused by an objective lens. The fluorescence collected by the objective lens is analyzed by the single-photon counting modules and the spectrometer, passing through the dichroic mirror, the long pass filter, and the beam splitter.

### 4. Experimental results

#### 4.1. Emission linewidth for SiV centers created in nanodiamonds

Here, we describe the experimental results for the nanodiamonds when the ion fluence was  $10^{13}$  ions/cm<sup>2</sup>. We determine the fluorescence of nanodiamonds from confocal scanning images. Figure 3(a) is a confocal scanning image of sample A. There are several bright spots with different intensity in the observed area. Figure 3(b) is the emission spectra of the bright spots in the confocal image, A-1, A-2, and A-3. Note that light with a wavelength of less than 722 nm is

blocked by the long pass filter. A sharp emission peak is observed at a wavelength of 738 nm for each spot, which corresponds to the ZPL of a SiV center in the diamond [8,9]. The linewidths for spot A-1 (black line) and spot A-2 (red line) are 9 nm and 7 nm, respectively. Note that when we measured the spectra of seven spots [three of them are shown in Fig. 3(b)], all of 7 spots showed SiV-related emission peak.

The measured confocal scanning image of sample B is shown in Fig. 3(c). There are several bright spots with different intensities in the observed area. Figure 3(d) is the emission spectra of B-1 and B-2. Spot B-1 (black line) shows a broad emission peak at a wavelength of 766 nm, which is almost in agreement with the peak wavelength of the phonon side band for SiV centers [9]. Spot B-2 (red line) shows a sharp emission peak with a linewidth of 10 nm at a wavelength of 738 nm.

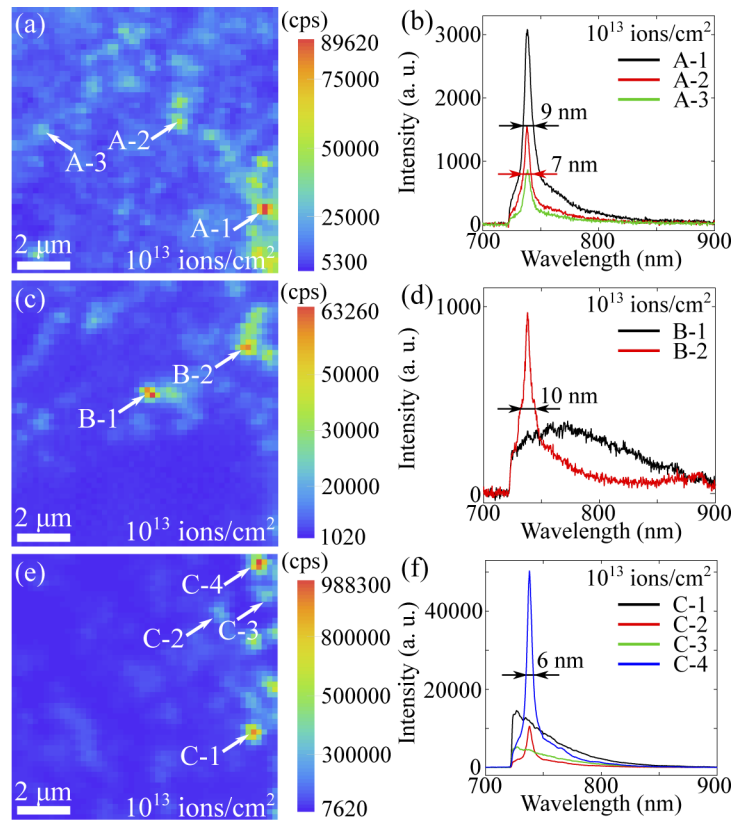


**Fig. 3.** Scanning confocal images [(a), (c), and (e)] and emission spectra [(b), (d), and (f)] at an ion fluence of  $10^{13}$  ions/cm<sup>2</sup>. (a) and (b) Results for sample A. (c) and (d) Results for sample B. (e) and (f) Results for sample C.

Figure 3(f) is the emission spectra of sample C at the bright spots (C-1, C-2, C-3, and C-4) in Fig. 3(e). Spots of C-2 (red line) and C-4 (blue line) show SiV ZPL centers at a wavelength of about 738 nm. The linewidth for the ZPL of C-4 is 6 nm.

Next, we investigate the nanodiamonds when the ion fluence is increased to  $2 \times 10^{15}$  ions/cm<sup>2</sup>. Figure 4(a) is a confocal image of sample B. Figure 4(b) is the emission spectra of the bright spots B-3, B-4, and B-5 in Fig. 4(a). Spots B-3 (black line) and B-5 (green line) show sharp peaks associated with the SiV centers at a wavelength of 739 nm. The linewidth for the emission peak of B-5 is 10 nm, which is slightly broader than that for the ion fluence of  $10^{13}$  ions/cm<sup>2</sup>.

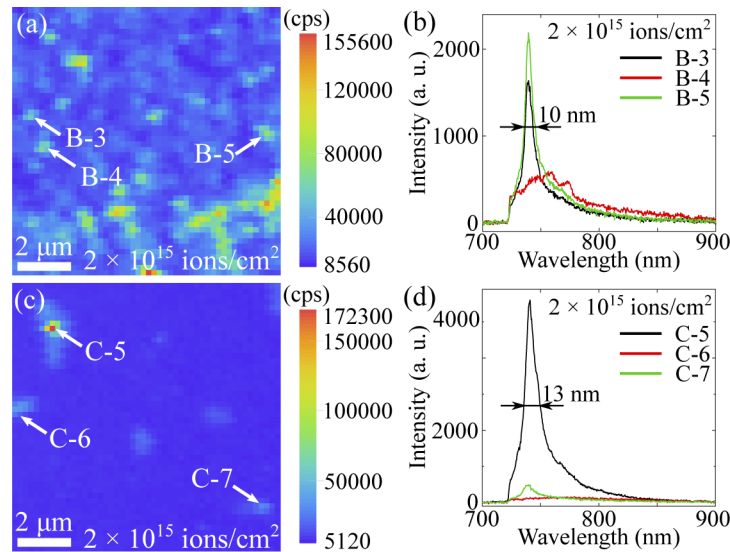


**Fig. 4.** Scanning confocal images [(a) and (c)] and emission spectra [(b) and (d)] at an ion fluence of  $2 \times 10^{15}$  ions/cm<sup>2</sup>. (a) and (b) Results for sample B. (c) and (d) Results for sample C.

We measured a confocal image and emission spectrum for sample C. Figure 4(d) is the emission spectra of the bright spots C-5, C-6, and C-7. Spot C-5 (black line) produces a sharp emission peak due to SiV centers at a wavelength of 740 nm. The linewidth for this peak is 13 nm, which is broader than for an ion fluence of  $10^{13}$  ions/cm<sup>2</sup>. Spot C-7 (green line) also shows a sharp emission peak with a linewidth of 15 nm at a wavelength of 739 nm. The broadening of the ZPL peaks and the red shifts are likely to be due to an increase in the strain in the nanodiamonds and degradation of the crystal quality by the high ion fluence [37].

Note that we observed no narrow emission peaks related to SiV centers for sample A. This is likely due to deterioration of the crystal quality of the nanodiamonds by the high-fluence ion implantation.

For an ion fluence of  $10^{11}$  ions/cm<sup>2</sup>, we do not observe any sharp emission peaks due to SiV centers in any of the samples (see Appendix).

The ZPL linewidths for the measured SiV centers were distributed in the range of 6–15 nm. These are slightly broader than those (about 4 nm) for SiV centers in unstrained bulk diamond [45]. However, the distribution range is almost the same as the distribution of ZPL linewidths for SiV centers in nanodiamonds produced by the CVD method [36,37,42]. Therefore, we believe that the SiV centers in the nanodiamonds produced by ion implantation have a quality as good as in these large nanodiamonds.

To investigate the effect of high-temperature annealing, we measured samples annealed at 800°C (first step of the annealing method). For this purpose, we used sample C. For an ion fluence of  $10^{13}$  ions/cm<sup>2</sup>, emission peaks at around 740 nm were observed from only three bright spots out of the measured 40 bright spots. The narrowest linewidth observed for a bright spot was 12.8 nm, which is more than twice as broad as the linewidth for a nanodiamond annealed at 1100°C, as shown in Fig. 3(f). For an ion fluence of  $2 \times 10^{15}$  ions/cm<sup>2</sup>, broad emission peaks at around 740 nm were observed for all 20 measured bright spots. However, the average linewidth is  $22.3 \pm 4.1$  nm, which is broader than the case for annealing at 1100°C, as shown in Fig. 4(d). From these results, we believe that high-temperature annealing at 1100°C plays a key role in the formation of SiV centers with narrow linewidths.

#### 4.2. Estimation of the number of SiV centers

In order to investigate the number of SiV centers, we measure the second-order correlation function  $g^2(\tau)$ . As a sample for this measurement, we use sample B with an ion fluence of  $10^{13}$  ions/cm<sup>2</sup>. Note that this is different from the sample used in the above experiments [Fig. 3(c) and Fig. 3(d)]. Figure 5(a) is the emission spectrum of the measured nanodiamond. The black line shows the experimental results with the background emission subtracted. A sharp emission peak at 737 nm is observed together with a broad emission peak. The red line shows the fitting results when two emission spectra (blue and green lines) are assumed, and agrees well with the experimental results. We measured the second-order correlation function  $g^2(\tau)$  for this nanodiamond as shown in Fig. 5(b). The black line shows the experimental results with background correction when the signal and the background counts are 59200 counts/s and 8300 counts/s, respectively. A sharp dip is observed at around zero delay. The blue line shows the fitting results when using Eq. (1).

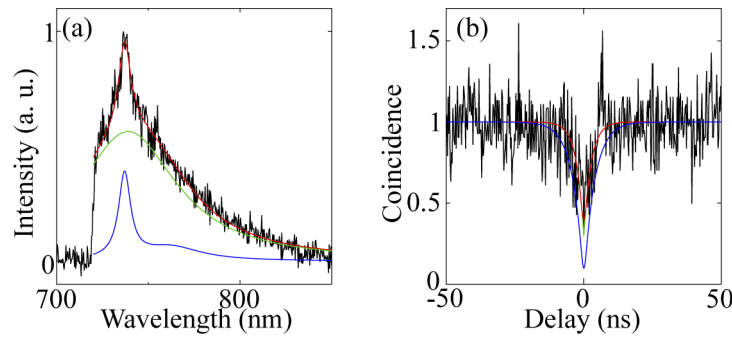


**Fig. 5.** (a) Emission spectrum of sample B with an ion fluence of  $10^{13}$  ions/cm<sup>2</sup>. The black line shows the experimental results and the red line shows the fitting results for two emission spectra (green and blue lines). (b) Second-order photon correlation. The black line shows the experimental results and the red line shows the fitting results. The green line shows the calculation results with the influence of the timing jitter deconvoluted from the fitting results (red line). The blue line shows the fitting results when using Eq. (1).

Taking into account the timing jitter of the detection system, which has a Gaussian shape, the correlation function  $g_i^2(\tau)$  for a defect center with a two-level system is expressed as

$$g_i^2(\tau) = \int_{-\infty}^{\infty} \frac{1}{\sqrt{2\pi}\sigma} e^{-\frac{1}{2}\left(\frac{t}{\sigma}\right)^2} (1 - e^{-\frac{|t|}{\tau_i}}) dt. \quad (1)$$

Here,  $\sigma$  is determined to be 521 ps from pulse laser measurements with a pulse length of 40 ps. Note that a two-level system can be used since no bunching behavior was observed in the experimental results. The blue line in Fig. 5(b) shows the fitting results using this equation, and does not agree with the experimental results.

As the next step, we assume that there are two independent defect centers (defect 1 and 2) in the detection focal area. In this case,  $g^2(\tau)$  is given by [46]

$$g^2(\tau) = z^2 g_1^2(\tau) + (1-z)^2 g_2^2(\tau) + 2z(1-z). \quad (2)$$

Here  $g_{1,2}^2(\tau)$  is the correlation function for a single defect center given by Eq. (1).  $z$  is the relative intensity fraction for two defect centers, which is determined to be 0.82 from the integrated ratio of two estimated emission spectra (green and blue lines) in Fig. 5(a). The red line in Fig. 5(b) shows the fitting results using Eq. (2). This is in good agreement with the experimental results. The green line shows the calculation results when the timing jitter is assumed to be zero and  $g^2(0)$  is estimated to be 0.3.

For several other tens of spots for sample A and B with an ion fluence of  $10^{13}$  ions/cm<sup>2</sup>, we were not able to observe dips in  $g^2(\tau)$ . This would be due to the fact that the amount of implanted ions was higher than that required for the creation of a single SiV center. Note that no SiV centers were created in nanodiamonds when an ion fluence was  $10^{11}$  ions/cm<sup>2</sup>.

## 5. Conclusion

In conclusion, we have fabricated nanodiamonds containing SiV centers with narrow ZPLs, which had previously been difficult to achieve by ion implantation. Si ions were implanted into the nanodiamonds with three different median sizes,  $29.9 \pm 16.0$  nm,  $53.7 \pm 11.2$  nm, and  $65.7 \pm 28.8$  nm. After the implantation, the samples were treated by high-temperature and high-vacuum annealing. For an ion fluence of  $10^{13}$  ions/cm<sup>2</sup>, SiV centers with a narrow linewidth of 7 nm at room temperature were found in nanodiamonds with a median size of  $29.9 \pm 16.0$  nm. Moreover, we observed a dip in the second-order correlation function  $g^2(\tau)$  for Si-implanted nanodiamonds with a median size of 50 nm for the first time, to the best of our knowledge. Taking into account the timing jitter of our detection system and the two defect centers, it was possible to reproduce the measured  $g^2(\tau)$ .  $g^2(0)$  without timing jitter was estimated to be 0.3. Creating single SiV centers in nanodiamonds by optimizing the ion fluence and evaluating optical properties at low temperature will be a subject of future work. Our process of implanting and transferring silicon ions in nanodiamonds provides a route towards novel biomarkers for life-science, nanoscale thermometry, and nanophotonic quantum information devices.

## Appendix: Experimental results for an ion fluence of $10^{11}$ ions/cm<sup>2</sup>

We measured nanodiamonds with an ion fluence of  $10^{11}$  ions/cm<sup>2</sup>. Figure 6(a) is a confocal scanning image for sample A. There are several bright spots in the measured area. We measured the emission spectra of the bright spots indicated by the arrows and numbers as shown in Fig. 6(b). All the spots show emission spectra with three peaks at wavelengths of 725 nm, 758 nm, and 773 nm. The peak wavelength of 725 nm is almost in agreement with the emission peak for C-1 in Fig. 3(f), while the peaks at 758 nm and 773 nm are not observed for ion fluences of  $10^{13}$  ions/cm<sup>2</sup> and  $10^{15}$  ions/cm<sup>2</sup>.

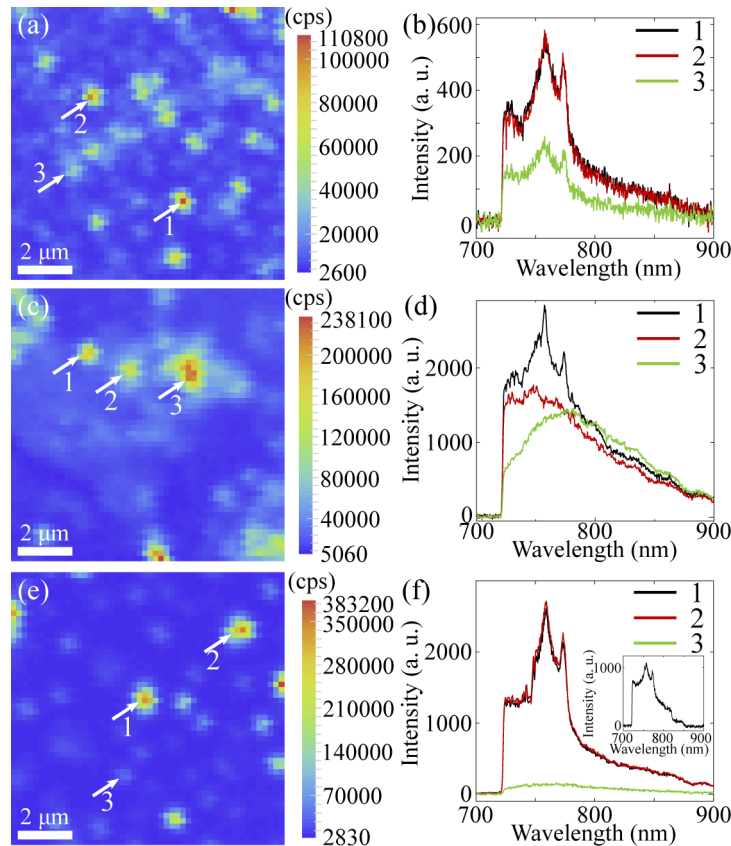
Figure 6(c) is a confocal scanning image for sample B. This sample also has several bright spots. Note that the slight blurring of the image is due to a slight misalignment of the optical setup. Figure 6(d) is the emission spectra of the bright spots indicated by the arrows and numbers. Line 1 (black line) shows three peaks, as for the nanodiamonds for sample A. Line 2 (red line) shows a broad spectrum with a peak at a wavelength of 748 nm. Line 3 (green line) shows a broad spectrum with a peak at a wavelength of 778 nm.

Figure 6(e) is a confocal scanning image for sample C. There are several bright spots in the measured area. Figure 6(f) shows emission spectra of the bright spots indicated by the arrows and numbers. Lines 1 (black line) and 2 (red line) show emission spectra with three peaks. Line 3 shows a weak, broad emission peak at a wavelength of 760 nm. Although we measured other samples, we could not observe any sharp emission peaks due to SiV centers for an ion fluence of  $10^{11}$  ions/cm<sup>2</sup>.

To clarify whether the spectra with three peaks are related to silicon ions, we measure nanodiamonds without ion implantation and annealing at high temperature in vacuum. The inset of Fig. 6(f) is the emission spectrum of sample C. Three peaks are clearly observed in the spectrum. We also observe a similar spectrum with three peaks for a nanodiamond annealed at high temperature without ion implantation. These results indicate that the emission spectrum with three peaks is not due to silicon ions but to other impurities such as nitrogen originally contained in the nanodiamonds used in this study.

**Funding.** Japan Society for the Promotion of Science (16K04918, 19K03686, 19K03700, 26220712, 21H04444);





**Fig. 6.** For an ion fluence of  $10^{11}$  ions/cm<sup>2</sup>, scanning confocal images [(a), (c), and (e)] and emission spectra [(b), (d), and (f)]. (a) and (b) results for sample A. (c) and (d) results for sample B. (e) and (f) results for sample C. The inset of (f) is an emission spectrum for nanodiamonds without ion implantation and annealing.

Core Research for Evolutional Science and Technology (JPMJCR1674); the MEXT Quantum Leap Flagship Program (MEXT Q-LEAP) (JPMXS0118067634); Matsuo Foundation.

**Acknowledgments.** We wish to thank Prof. Mitsuaki Kaneko at Kyoto University for SEM measurements. We gratefully acknowledge financial support in the form of Kakenhi Grants-in-Aid (Nos. 21H04444, 26220712, 16K04918, 19K03700, and 19K03686) from the Japan Society for the Promotion of Science (JSPS), the CREST program of the Japan Science and Technology Agency (JST) (JPMJCR1674), and the MEXT Quantum Leap Flagship Program (MEXT Q-LEAP) (JPMXS0118067634). H. T. acknowledges the support of the Matsuo Foundation.

**Disclosures.** The authors declare no conflicts of interest.

**Data availability.** Data underlying the results presented in this paper are not publicly available at this time but may be obtained from the authors upon reasonable request.

## References

1. S. W. Hell and J. Wichmann, "Breaking the diffraction resolution limit by stimulated emission: stimulated-emission-depletion fluorescence microscopy," *Opt. Lett.* **19**(11), 780–782 (1994).
2. E. Betzig, "Proposed method for molecular optical imaging," *Opt. Lett.* **20**(3), 237–239 (1995).
3. J. R. Maze, P. L. Stanwix, J. S. Hodges, S. Hong, J. M. Taylor, P. Cappellaro, L. Jiang, M. V. G. Dutt, E. Togan, A. S. Zibrov, A. Yacoby, R. L. Walsworth, and M. D. Lukin, "Nanoscale magnetic sensing with an individual electronic spin in diamond," *Nature* **455**(7213), 644–647 (2008).
4. P. Maletinsky, S. Hong, M. S. Grinolds, B. Hausmann, M. D. Lukin, R. L. Walsworth, M. Loncar, and A. Yacoby, "A robust scanning diamond sensor for nanoscale imaging with single nitrogen-vacancy centres," *Nat. Nanotechnol.* **7**(5), 320–324 (2012).

5. G. Kucsko, P. C. Maurer, N. Y. Yao, M. Kubo, H. J. Noh, P. K. Lo, H. Park, and M. D. Lukin, "Nanometre-scale thermometry in a living cell," *Nature* **500**(7460), 54–58 (2013).
6. J. Wrachtrup and F. Jelezko, "Processing quantum information in diamond," *J. Phys.: Condens. Matter* **18**(21), S807–S824 (2006).
7. Z.-L. Xiang, S. Ashhab, J. Q. You, and F. Nori, "Hybrid quantum circuits: Superconducting circuits interacting with other quantum systems," *Rev. Mod. Phys.* **85**(2), 623–653 (2013).
8. E. Neu, D. Steinmetz, J. Riedrich-Möller, S. Gsell, M. Fischer, M. Schreck, and C. Becher, "Single photon emission from silicon-vacancy colour centres in chemical vapour deposition nano-diamonds on iridium," *New J. Phys.* **13**(2), 025012 (2011).
9. A. Sipahigil, K. D. Jahnke, L. J. Rogers, T. Teraji, J. Isoya, A. S. Zibrov, F. Jelezko, and M. D. Lukin, "Indistinguishable photons from separated silicon-vacancy centers in diamond," *Phys. Rev. Lett.* **113**(11), 113602 (2014).
10. L. J. Rogers, K. D. Jahnke, T. Teraji, L. Marseglia, C. Müller, B. Naydenov, H. Schauffert, C. Kranz, J. Isoya, L. P. McGuinness, and F. Jelezko, "Multiple intrinsically identical single-photon emitters in the solid state," *Nat. Commun.* **5**(1), 4739 (2014).
11. T. Schröder, M. E. Trusheim, M. Walsh, L. Li, J. Zheng, M. Schukraft, A. Sipahigil, R. E. Evans, D. D. Sukachev, C. T. Nguyen, J. L. Pacheco, R. M. Camacho, E. S. Bielejec, M. D. Lukin, and D. Englund, "Scalable focused ion beam creation of nearly lifetime-limited single quantum emitters in diamond nanostructures," *Nat. Commun.* **8**(1), 15376 (2017).
12. B. Kambs and C. Becher, "Limitations on the indistinguishability of photons from remote solid state sources," *New J. Phys.* **20**(11), 115003 (2018).
13. K. Li, Y. Zhou, A. Rasmita, I. Aharonovich, and W. B. Gao, "Nonblinking emitters with nearly lifetime-limited linewidths in CVD nanodiamonds," *Phys. Rev. Appl.* **6**(2), 024010 (2016).
14. J. N. Becker, B. Pingault, D. Groß, M. Gündoğan, N. Kukharchyk, M. Markham, A. Edmonds, M. Atatüre, P. Bushev, and C. Becher, "All-optical control of the silicon-vacancy spin in diamond at millikelvin temperatures," *Phys. Rev. Lett.* **120**(5), 053603 (2018).
15. T. Müller, C. Hepp, B. Pingault, E. Neu, S. Gsell, M. Schreck, H. Sternschulte, D. Steinmüller-Nethl, C. Becher, M. Atatüre, T. Mu, C. Hepp, B. Pingault, E. Neu, S. Gsell, M. Schreck, C. Becher, and M. Atatu, "Optical signatures of silicon-vacancy spins in diamond," *Nat. Commun.* **5**(1), 3328 (2014).
16. L. J. Rogers, K. D. Jahnke, M. H. Metsch, A. Sipahigil, J. M. Binder, T. Teraji, H. Sumiya, J. Isoya, M. D. Lukin, P. Hemmer, and F. Jelezko, "All-optical initialization, readout, and coherent preparation of single silicon-vacancy spins in diamond," *Phys. Rev. Lett.* **113**(26), 263602 (2014).
17. D. D. Sukachev, A. Sipahigil, C. T. Nguyen, M. K. Bhaskar, R. E. Evans, F. Jelezko, and M. D. Lukin, "Silicon-vacancy spin qubit in diamond: a quantum memory exceeding 10 ms with single-shot state readout," *Phys. Rev. Lett.* **119**(22), 223602 (2017).
18. I. A. Khramtsov and D. Y. Fedyanin, "Bright single-photon emitting diodes based on the silicon-vacancy center in AlN/diamond heterostructures," *Nanomaterials* **10**(2), 361 (2020).
19. J. Riedrich-Möller, C. Arend, C. Pauly, F. Mücklich, M. Fischer, S. Gsell, M. Schreck, and C. Becher, "Deterministic coupling of a single silicon-vacancy color center to a photonic crystal cavity in diamond," *Nano Lett.* **14**(9), 5281–5287 (2014).
20. A. Sipahigil, R. E. Evans, D. D. Sukachev, M. J. Burek, J. Borregaard, M. K. Bhaskar, C. T. Nguyen, J. L. Pacheco, H. A. Atikian, C. Meuwly, R. M. Camacho, F. Jelezko, E. Bielejec, H. Park, M. Lončar, and M. D. Lukin, "An integrated diamond nanophotonics platform for quantum-optical networks," *Science* **354**(6314), 847–850 (2016).
21. J. Wolters, A. W. Schell, G. Kewes, N. Nüsse, M. Schoengen, H. Döschner, T. Hannappel, B. Löchel, M. Barth, and O. Benson, "Enhancement of the zero phonon line emission from a single nitrogen vacancy center in a nanodiamond via coupling to a photonic crystal cavity," *Appl. Phys. Lett.* **97**(14), 141108 (2010).
22. B.-S. Song, S. Noda, T. Asano, and Y. Akahane, "Ultra-high-Q photonic double-heterostructure nanocavity," *Nat. Mater.* **4**(3), 207–210 (2005).
23. M. Fujiwara, K. Toubaru, T. Noda, H.-Q. Zhao, and S. Takeuchi, "Highly efficient coupling of photons from nanoemitters into single-mode optical fibers," *Nano Lett.* **11**(10), 4362–4365 (2011).
24. R. Yalla, F. Le Kien, M. Morinaga, and K. Hakuta, "Efficient channeling of fluorescence photons from single quantum dots into guided modes of optical nanofiber," *Phys. Rev. Lett.* **109**(6), 063602 (2012).
25. T. Schröder, M. Fujiwara, T. Noda, H.-Q. Zhao, O. Benson, and S. Takeuchi, "A nanodiamond-tapered fiber system with high single-mode coupling efficiency," *Opt. Express* **20**(10), 10490–10497 (2012).
26. M. Fujiwara, K. Yoshida, T. Noda, H. Takashima, A. W. Schell, N. Mizuochi, and S. Takeuchi, "Manipulation of single nanodiamonds to ultrathin fiber-taper nanofibers and control of NV-spin states toward fiber-integrated  $\lambda$ -systems," *Nanotechnology* **27**(45), 455202 (2016).
27. A. W. Schell, H. Takashima, T. T. Tran, I. Aharonovich, and S. Takeuchi, "Coupling quantum emitters in 2D materials with tapered fibers," *ACS Photonics* **4**(4), 761–767 (2017).
28. A. W. Schell, H. Takashima, S. Kamioka, Y. Oe, M. Fujiwara, O. Benson, and S. Takeuchi, "Highly Efficient Coupling of Nanolight Emitters to a Ultra-Wide Tunable Nanofiber Cavity," *Sci. Rep.* **5**(1), 9619 (2015).
29. H. Takashima, M. Fujiwara, A. W. Schell, and S. Takeuchi, "Detailed numerical analysis of photon emission from a single light emitter coupled with a nanofiber Bragg cavity," *Opt. Express* **24**(13), 15050–15058 (2016).

30. W. Li, J. Du, and S. Nic Chormaic, "Tailoring a nanofiber for enhanced photon emission and coupling efficiency from single quantum emitters," *Opt. Lett.* **43**(8), 1674–1677 (2018).
31. H. Takashima, A. Fukuda, H. Maruya, T. Tashima, A. W. Schell, and S. Takeuchi, "Fabrication of a nanofiber Bragg cavity with high quality factor using a focused helium ion beam," *Opt. Express* **27**(5), 6792 (2019).
32. P. Romagnoli, M. Maeda, J. M. Ward, V. G. Truong, and S. Nic Chormaic, "Fabrication of optical nanofibre-based cavities using focussed ion-beam milling: a review," *Appl. Phys. B: Lasers Opt.* **126**(6), 111 (2020).
33. A. W. Schell, G. Kewes, T. Schröder, J. Wolters, T. Aichele, and O. Benson, "A scanning probe-based pick-and-place procedure for assembly of integrated quantum optical hybrid devices," *Rev. Sci. Instrum.* **82**(7), 073709 (2011).
34. C. T. Nguyen, R. E. Evans, A. Sipahigil, M. K. Bhaskar, D. D. Sukachev, V. N. Agafonov, V. A. Davydov, L. F. Kulikova, F. Jelezko, and M. D. Lukin, "All-optical nanoscale thermometry with silicon-vacancy centers in diamond," *Appl. Phys. Lett.* **112**(20), 203102 (2018).
35. H. Zhang, I. Aharonovich, D. R. Glenn, R. Schalek, A. P. Magyar, J. W. Lichtman, E. L. Hu, and R. L. Walsworth, "Silicon-vacancy color centers in nanodiamonds: cathodoluminescence imaging markers in the near infrared," *Small* **10**(10), 1908–1913 (2014).
36. E. Neu, C. Arend, E. Gross, F. Guldner, C. Hepp, D. Steinmetz, E. Zscherpel, S. Ghodbane, H. Sternschulte, D. Steinmüller-Nethl, Y. Liang, A. Krueger, and C. Becher, "Narrowband fluorescent nanodiamonds produced from chemical vapor deposition films," *Appl. Phys. Lett.* **98**(24), 243107 (2011).
37. S. Lindner, A. Bommer, A. Muzha, A. Krueger, L. Gines, S. Mandal, O. Williams, E. Londero, A. Gali, and C. Becher, "Strongly inhomogeneous distribution of spectral properties of silicon-vacancy color centers in nanodiamonds," *New J. Phys.* **20**(11), 115002 (2018).
38. U. Jantzen, A. B. Kurz, D. S. Rudnicki, C. Schäfermeier, K. D. Jahnke, U. L. Andersen, V. A. Davydov, V. N. Agafonov, A. Kubanek, L. J. Rogers, and F. Jelezko, "Nanodiamonds carrying silicon-vacancy quantum emitters with almost lifetime-limited linewidths," *New J. Phys.* **18**(7), 073036 (2016).
39. S. V. Bolshedvorskii, A. I. Zelenev, V. V. Vorobyov, V. V. Soshenko, O. R. Rubinas, L. A. Zhulikov, P. A. Pivovarov, V. N. Sorokin, A. N. Smolyaninov, L. F. Kulikova, A. S. Garanina, S. G. Lyapin, V. N. Agafonov, R. E. Uzbekov, V. A. Davydov, and A. V. Akimov, "Single silicon vacancy centers in 10 nm diamonds for quantum information applications," *ACS Appl. Nano Mater.* **2**(8), 4765–4772 (2019).
40. T. D. Merson, S. Castelletto, I. Aharonovich, A. Turbic, T. J. Kilpatrick, and A. M. Turnley, "Nanodiamonds with silicon vacancy defects for nontoxic photostable fluorescent labeling of neural precursor cells," *Opt. Lett.* **38**(20), 4170 (2013).
41. H. Kim, H. Kim, J. Lee, W. C. Lim, J. A. Eliades, J. Kim, J. Song, and J. Suk, "Fabrication of silicon-vacancy color centers in nanodiamonds by using Si-ion implantation," *J. Korean Phys. Soc.* **73**(5), 661–666 (2018).
42. C. K. Chen, Y. S. Mei, J. M. Cui, X. Li, M. Y. Jiang, S. H. Lu, and X. J. Hu, "Man-made synthesis of ultrafine photoluminescent nanodiamonds containing less than three silicon-vacancy colour centres," *Carbon* **139**, 982–988 (2018).
43. R. E. Evans, A. Sipahigil, D. D. Sukachev, A. S. Zibrov, and M. D. Lukin, "Narrow-linewidth homogeneous optical emitters in diamond nanostructures via silicon ion implantation," *Phys. Rev. Appl.* **5**(4), 044010 (2016).
44. H. Takashima, H. Maruya, K. Ishihara, T. Tashima, K. Shimazaki, A. W. Schell, T. T. Tran, I. Aharonovich, and S. Takeuchi, "Determination of the dipole orientation of single defects in hexagonal boron nitride," *ACS Photonics* **7**(8), 2056–2063 (2020).
45. C. Arend, J. N. Becker, H. Sternschulte, D. Steinmüller-Nethl, and C. Becher, "Photoluminescence excitation and spectral hole burning spectroscopy of silicon vacancy centers in diamond," *Phys. Rev. B* **94**(4), 045203 (2016).
46. A. Bommer and C. Becher, "New insights into nonclassical light emission from defects in multi-layer hexagonal boron nitride," *Nanophotonics* **8**(11), 2041–2048 (2019).